
History Matching of Reservoir Models by Ensemble Kalman Filtering: The State of the Art and a Sensitivity Study

Leila Heidari, Véronique Gervais, and Mickaële Le Ravalec

IFP Energies nouvelles, Reservoir Engineering Department, Rueil Malmaison, France

Hans Wackernagel

Geostatistics Group, Centre de Géosciences, MINES ParisTech, Fontainebleau, France

ABSTRACT

History matching is to integrate dynamic data in the reservoir model–building process. These data, acquired during the production life of a reservoir, can be production data, such as well pressures, oil production rates or water production rates, or four-dimensional seismic-related data. The ensemble Kalman filter (EnKF) is a sequential history-matching method that integrates the production data to the reservoir model as soon as they are acquired. Its ease of implementation and efficiency has resulted in various applications, such as history matching of production and seismic data.

We focus on the use of the EnKF for history match of a synthetic reservoir model. First, the method of ensemble Kalman filtering is reviewed. Then the geologic and reservoir characteristics of a case study are described. Several experiments are performed to investigate the benefits and limitations of the EnKF approach in building reservoir models that reproduce the production data. Last, special attention is paid to the sensitivity of the method to a set of parameters, including ensemble size, assimilation time interval, data uncertainty, and choice of initial ensemble.

INTRODUCTION

A reservoir model relies on two sources of data: static data and dynamic data. Although static data (e.g., geologic observations, measurements on cores, logs, etc.) are constant through time, dynamic data change with time. They include production data measured at wells, such as pressures and oil production rates. As static data are too sparse to deterministically describe the spa-

tial variation in transport properties (porosity and permeability) within the reservoir, they serve to characterize the parameters of a geostatistical model. Therefore, we refer to a stochastic framework in which reservoir models are viewed as realizations of a random function.

Accounting for dynamic data in reservoir models is not straightforward, and this process is known as “history matching” in the literature. It consists of building a numerical reservoir model, which consists of a

grid populated by porosity and permeability values that reproduce the production behavior observed in the field. Among the various methods proposed for performing history matching, the ensemble Kalman filter (EnKF) has recently provided promising results in terms of reservoir characterization and uncertainty quantification. It has been widely used in different fields, such as oceanography (Haugen and Evensen, 2002), meteorology (Evensen and van Leeuwen, 1996), hydrology (Margulis et al., 2002), and petroleum engineering (Naevdal et al., 2002).

The EnKF is a variation of the well-known KF (Kalman, 1960) for dealing with highly nonlinear problems (Evensen, 1994), as is the case of fluid flow in porous media. These filters represent, with error covariance matrices, the uncertainties in the reservoir model, with respect to properties such as porosity, permeability, pressure, saturation, and so on. The model and its uncertainties are propagated through time according to a dynamic system describing fluid flow in porous media. Whenever measurements are available, a new estimate for the model and its uncertainties is calculated by a variance minimization scheme (Evensen, 2007).

Kalman filters are sequential, meaning that the available dynamic data are sequentially integrated in the modeling as soon as they are obtained. Time is divided into successive steps or assimilation intervals; each time step begins at the end of the previous one and lasts until the next measurements are available. During each time step, the filter acts according to two stages. The first stage is forecasting: its purpose is to propagate the reservoir model by running the flow simulation through the time step of interest. The second stage is analysis (or updating): the reservoir model is updated by adjusting the numerical flow responses with the measurements.

In the EnKF, the model uncertainties are represented by an ensemble, that is, a group, of realizations for model parameters and for model states. Model parameters are properties such as porosity and permeability that do not change with time, whereas model states are properties such as pressure and saturations that do change with time. The mathematical formulation of the EnKF (Evensen, 2007) requires the computation of the first and second statistical moments, that is, mean and variance for the reservoir parameters and states that are derived from an empirical average over a finite-size ensemble of realizations.

Several EnKF applications illustrate the method's merits and shortcomings that motivated the current efforts to improve filter performance. The first application of the EnKF in petroleum engineering was presented by Naevdal et al. (2002) on a two-dimensional near-well reservoir model, where permeability mod-

els were predicted. The EnKF proved to provide better parameter estimations and, consequently, improved predictions. Gu and Oliver (2005) applied EnKF to the three-dimensional PUNQ-S3 model. They found the EnKF method more efficient than other history-matching methods in terms of computational burden. In the literature, there exist similar applications of the EnKF on the PUNQ-S3 test case (Lorentzen et al., 2005; Gao et al., 2006). The EnKF was also applied to a facies history match by Liu and Oliver (2005), who concluded that the EnKF was more computationally efficient and easier to use than gradient-based minimization methods. Real field history matching using the EnKF was performed by Haugen et al. (2008) and Evensen et al. (2007), who consider the EnKF to provide a powerful history-matching method. Although the EnKF is generally regarded as a successful method of data assimilation, several scientists (Floris et al., 2001; PUNQ-S3 test case, 2010) have sought to improve its performance. These improvements concern several assumptions in the mathematical formulation of the filter that are not satisfied in practical applications. The four following paragraphs provide an overview of the main problems and corresponding proposals.

The EnKF relies on the use of a finite ensemble to describe the model uncertainties. However, this may lead to spurious correlations in the covariance matrix; unexpected high correlations can be observed for the points located far from observation points. In the atmospheric data assimilation literature (Hamill and Whitaker, 2001; Houtekamer and Mitchell, 2001), a distance-dependent correlation function is used to condition the covariance matrix. The idea is to limit the effect of each observation by considering a cutoff radius beyond which the correlations are negligible. Devegowda et al. (2007) performed a covariance localization based on a streamline-derived function. Its advantage is to relate the localization function directly to the physics of flow in porous media. Anderson (2001) discussed the sampling error inherent in the EnKF and suggested, as a simple remedy, to multiply the covariance matrix by a small factor, slightly larger than 1. More sophisticated methods dealing with the problem of spurious correlations can be found in Anderson (2007), Wang et al. (2007), and Fertig et al. (2007).

Another improvement concerns the Gaussian assumption for parameters and states in all KFs, including the EnKF. In reality, nature commonly departs from a Gaussian distribution. For instance, parameters such as permeability or state variables like water saturations commonly do not approximate a Gaussian distribution. In addition, even if the initial distributions are Gaussian, the nonlinearity of the dynamic model, that is, the fluid-flow equations, may result in non-Gaussian

distributions (Chen et al., 2009). Zafari and Reynolds (2007) applied EnKF to two simple nonlinear problems to investigate the two problems previously mentioned and concluded that the EnKF provides poor uncertainty characteristics when the Gaussian assumption is violated. Several methods were proposed (Bertino et al., 2003; Vabø et al., 2008; Moreno et al., 2008) to modify the EnKF algorithm so that the Gaussianity requirement is better satisfied.

Next, the use of KFs implies that a linear relationship exists between measurements and model parameters and states, but such an assumption does not hold in fluid flow in porous media (Gu and Oliver, 2007). Wen and Chen (2005) proposed to add a confirmation step after the updating step in the EnKF algorithm; after each updating step, the fluid-flow simulation is performed for the current time step with the set of updated model parameters so that the dynamic variables are consistent with the model parameters. Zafari and Reynolds (2007) reconsidered the confirmation step and found it inappropriate within the framework of the EnKF. They argued that even for a linear problem, the update of dynamic variables with confirming EnKF misses some terms obtained by previous time step updates. However, Liu and Oliver (2005) suggested an iterative process to respect the nonlinear constraints that occur when dealing with facies. Gu and Oliver (2007) suggested that the EnKF workflow be combined with Gauss-Newton iterations within each time step. This method is appropriate whenever the differences between the measurements and the corresponding numerical responses are large.

Last, in the EnKF method, a representative spread should be preserved between ensemble members to avoid excessive variance reduction or “inbreeding.” This can be achieved by increasing the size, that is, number of members, of an ensemble, but at the expense of higher computational costs. Houtekamer and Mitchell (1998) argued that inbreeding comes from the fact that the ensemble used to calculate the covariance matrix was also the one updated through the EnKF update step. Therefore, they suggested using two ensembles so that the covariance calculated from one ensemble was used to update the other ensemble and vice versa. Moreover, for small ensemble sizes, more coupled ensembles would be necessary.

In this chapter, we apply the EnKF for history matching a variant of the well-known reservoir model, PUNQ-S3 (Floris et al., 2001). We first present the reservoir case study and then the implementation of the EnKF to perform a history match of production data. Moreover, to assess the advantages and shortcomings of the EnKF, we perform a set of sensitivity tests and investigate the influence of parameters such as the size

of the ensemble, the uncertainty in the measurements, the assimilation time step, and the choice of the initial ensemble. Details on the mathematical formulation of the EnKF methodology can be found in Evensen (2007).

OVERVIEW OF THE PUNQ-S3 CASE

The PUNQ-S3 case study (PUNQ-S3 test case, 2010) is a standard small-size reservoir engineering model set up by the PUNQ project (Production forecasting with UNcertainty Quantification) and commonly used for performing benchmarks. It is based on a real field that has been operated by Elf Exploration and Production. A full description of this case study can be found on the PUNQ-S3 Web page (PUNQ-S3 test case, 2010) and in Floris et al. (2001).

Geologic Description

The PUNQ model encompasses five layers with different petrophysical properties because of various depositional environments whose main characteristics are summarized as follows:

1. Layers 1, 3, and 5 correspond to fluvial channels encased in flood-plain mudstone. They consist of a low-porosity shale matrix (porosity <5%) with linear streaks of high-porosity sand (porosity >20%). These two sandy and shaly facies are represented by an “effective” facies with good reservoir properties.
2. Layer 2 consists of marine or lagoonal shales with distal mouth bars. This results in a low-porosity shaly matrix (porosity <5%) with a few higher porosity patches. Again, an effective facies with poor reservoir properties is used to represent this layer.
3. Layer 4 is a lagoonal delta, encased in lagoonal clay. It results in a low-porosity matrix (porosity <5%) with a more intermediate porosity region (porosity ~15%). This layer is then populated by an effective facies with intermediate reservoir properties.

Reservoir Model

The numerical model is built over a $19 \times 28 \times 5$ grid. The dimensions of each grid block in the X and Y directions are $180 \times 180 \text{ m}^2$ ($1938 \times 1938 \text{ ft}^2$), and the thickness is defined according to the database data set. A total of 1761 active cells are present and the reservoir is produced from six wells named PRO-1, PRO-4, PRO-5, PRO-11, PRO-12, and PRO-15. Figure 1 displays the top structure (layer 5) and the six well locations.

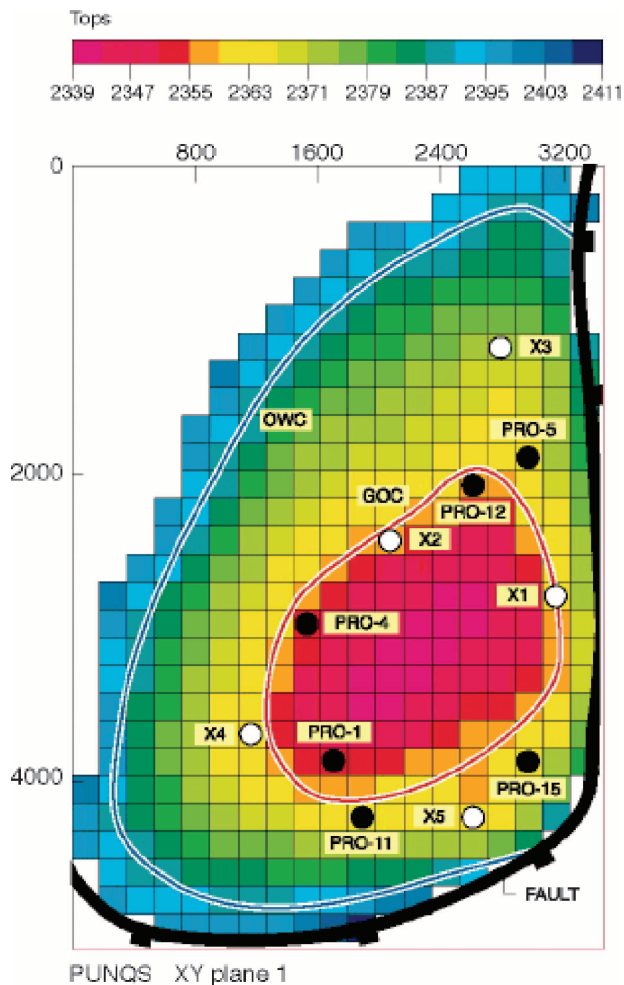


Figure 1. Top structure and well locations: PUNQ-S3 model from the PUNQ-S3 Web page (PUNQ-S3 test case, 2010). GOC = gas-oil contact; OWC = for oil-water contact.

The field is bounded by a fault to the east and south and by a strong aquifer to the west and north. Because of the strength of the aquifer, injection wells were not needed for pressure maintenance.

Petrophysical Properties

Porosity and horizontal permeability realizations are stochastically drawn to populate the five layers of the reservoir, and their statistical properties are reported in Table 1. Vertical permeability is assumed to be the same as the horizontal one. The data used to generate the realizations differed slightly from those provided by the PUNQ-S3 Web page (PUNQ-S3 test case, 2010) to enlarge the possible variations when performing sensitivity tests with the EnKF. In addition, the spatial variations in porosity and permeability are characterized

by a spherical variogram, whose main axes and anisotropy ratios are given in Table 1. All realizations (including the reference reservoir model) were generated on the basis of the fast Fourier transform moving average algorithm (Le Ravalec et al., 2000) without any conditioning to data at well locations. One of the resulting porosity and permeability models, which are used as the reference models in this study, is displayed in Figures 2 and 3.

Production Schedule

The original PUNQ-S3 case involves three-phase flows in the reservoir. In this chapter, we consider a simpler two-phase (oil and water) black-oil case, which has the advantage of providing more readable results. The original pressure-volume-temperature (PVT) data were modified to account for this change, whereas aquifer data remained unchanged. Relative permeability was generated according to the charts available in our database, and capillary pressure was assumed to be negligible. We kept a production schedule similar to the one developed for the original model, which is the same regardless of the production well. It consists of the following phases (Figure 4):

1. 1 yr of extended well testing with four 3-monthly production periods with production rates of 100, 200, 100, 50 m³/day, respectively;
2. 3 yr of well shut-in;
3. 4 yr of production; a well shut-in test is performed during the last 2 weeks of every year to collect shut-in pressure data. During the rest of the year, a constant production rate of 100 m³/day is set up.

Table 1. Facies properties.*

Layer	1	2	3	4	5
Facies	A	B	C	D	E
Porosity mean	0.1722	0.0802	0.1677	0.1615	0.1892
Porosity variance	0.0078	0.0004	0.0050	0.0006	0.0049
ln(kh) mean	2.18	1.41	2.24	2.47	2.49
ln(kh) variance	3.14	0.74	3.26	5.64	3.72
Correlation length (m)	3500	750	6000	1500	3750
First anisotropy ratio	0.286	1.0	0.25	0.50	0.333
Azimuth (degrees)	30	0	45	-30	60

*Porosity; logarithm of horizontal permeability, ln(kh); and variogram data.

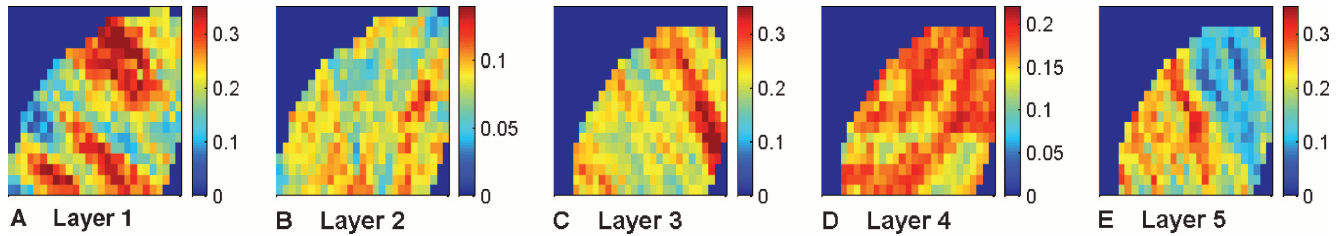


Figure 2. Reference porosity (in fractions) fields for the five layers in the model.

This flow rate constraint switches to a bottomhole pressure (BHP) constraint when pressure drops to 120 bars.

The study period spans between January 1, 1967, and January 15, 1975, that is, 8 yr, and it is referred to as the history-matching interval in the remainder of this chapter. The period is extended to July 1, 1983, to perform 8.5 yr of forecasting, and this additional period is termed the prediction interval. During the history-matching interval, measurements are obtained at irregular intervals. The noise levels that is, the standard deviations of the normal distribution defining the measurement uncertainties, were set to 2 bars for pressure, $2 \text{ m}^3/\text{day}$ for surface oil rate (SOR), and 0.02 for water cut (WCT).

HISTORY MATCH

We designed a twin experiment to investigate the usefulness of the EnKF for performing history match on our modified version of the PUNQ-S3 case. We followed the production schedule previously described to simulate production data during the history-matching interval for our reference reservoir model (Figures 2, 3): the resulting reference production data are the BHP, the SOR, and the WCT. The reference production data obtained for the six target producers yield the observations that need to be reproduced through the history-

matching process and they are shown for wells PRO-5 and PRO-15 in Figures 5 and 6, respectively (red curves).

The reference porosity and permeability fields are assumed to be unknown contrary to the reference production data and the primary purpose of the EnKF approach is to identify a set of realizations conditioned to these production data.

The history-matching intervals are split into 13 successive time steps, the end of each time step being associated to a change in the flow rate. These intervals or assimilation steps are displayed in Figure 4 on top of the expected SOR variations against time. For each time step, 18 reference data are available: 6 BHPs, 6 SORs, and 6 WCTs.

The size of the ensemble is set to 50: for each of the layers in the model, 50 realizations are generated for both porosity and permeability. These realizations have the same statistical properties (e.g., mean and variogram) as the reference reservoir model, whereas the other parameters, such as the relative permeability curves, the initial pressures, and the initial water saturations, are assumed to be known without uncertainty. Each ensemble member is updated according to the assimilation timing previously defined. This ensemble is denoted ensemble 1 in the following.

Because the number of active cells is 1761, 1761 unknown porosity and permeability values are present. Similarly, 1761 pressure and water saturation values are also present. Permeability and porosity are deemed as static parameters, whereas water saturation and pressure are dynamic variables, so that the state vector for

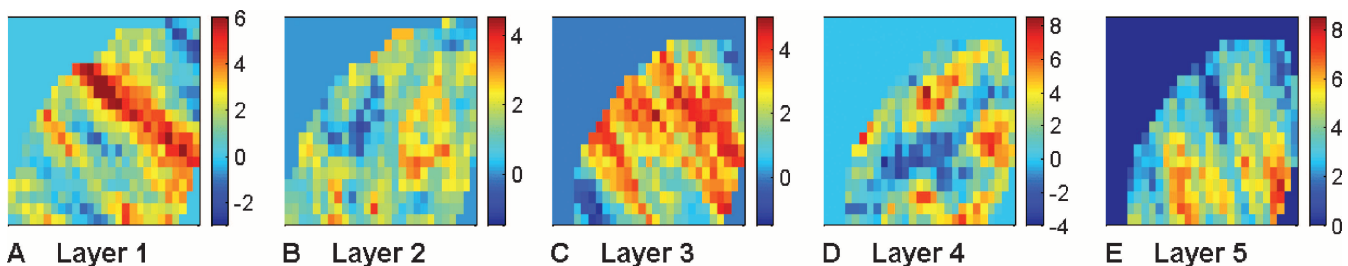


Figure 3. Logarithm of reference permeability (md) fields for the five layers in the model.

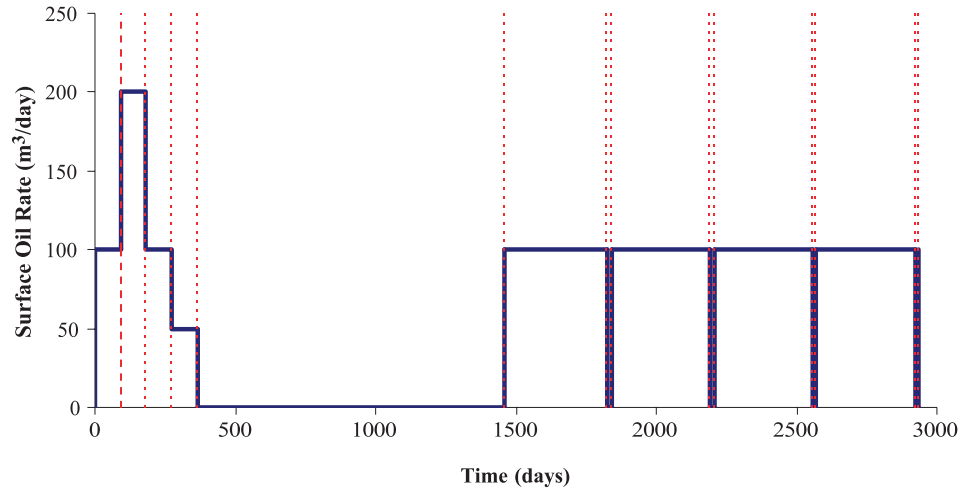


Figure 4. Evolution of the surface oil rate scheduled at the production wells during the history-matching interval. The vertical red lines indicate the assimilation times.

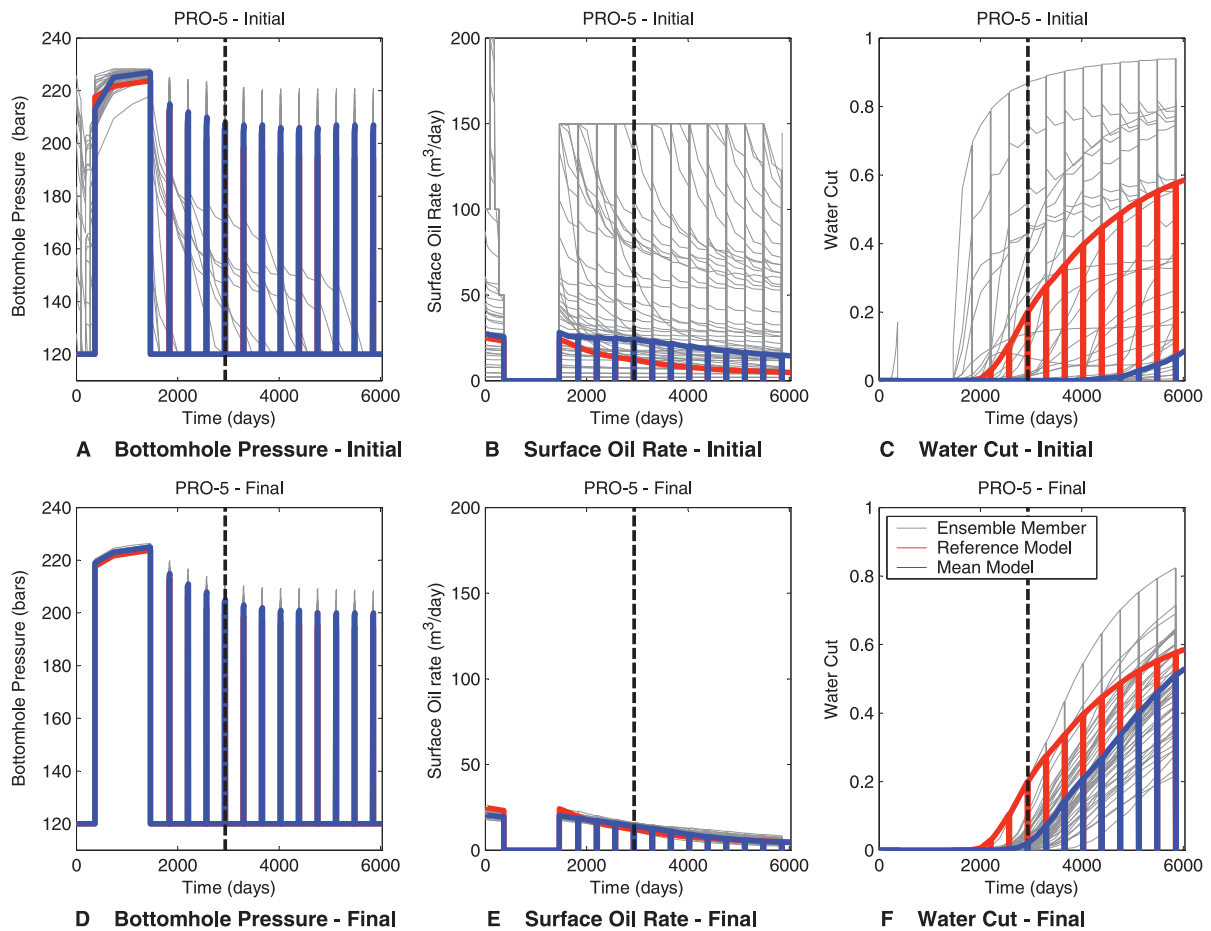


Figure 5. Production data simulated for well PRO-5 with an ensemble of size 50 during the history-matching and prediction periods. First row: Initial ensemble. Second row: Final ensemble updated with the ensemble Kalman filter. The black dashed vertical line at 2936 days indicates the time limit between the history-matching interval (0–2936 days) and the prediction interval (2936–6025 days). The gray curves correspond to the ensemble members, the red curves to the reference model, and the blue curves to the results obtained with the reservoir model computed as the mean of the ensemble.

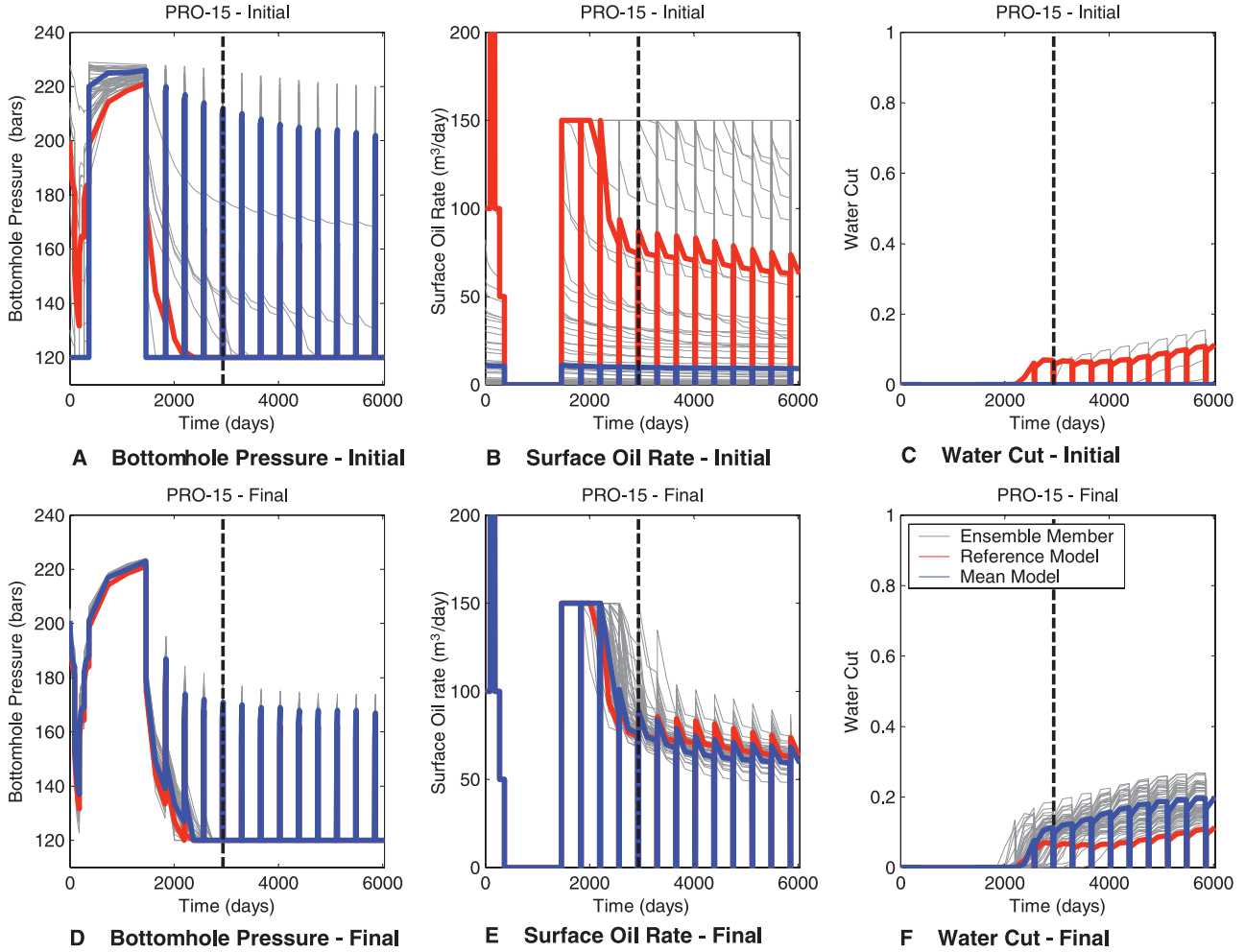


Figure 6. Production data simulated for well PRO-15 with an ensemble of size 50 during the history-matching and prediction periods. First row: Initial ensemble. Second row: Final ensemble updated with the ensemble Kalman filter. The black dashed vertical line at 2936 days indicates the time limit between the history-matching interval (0–2936 days) and the prediction interval (2936–6025 days). The gray curves correspond to the ensemble members, the red curves to the reference model, and the blue curves to the results obtained with the reservoir model computed as the mean of the ensemble.

the j^{th} ensemble member at the k^{th} time step is defined by

$$\begin{aligned} \psi_{k,j} = & [trans(\phi_{k,j,1}), \dots, trans(\phi_{k,j,N_a}), trans(kh_{k,j,1}), \dots, \\ & trans(kh_{k,j,N_a}), P_{k,j,1}, \dots, P_{k,j,N_a}, S_{wk,j,1}, \dots, \\ & S_{wk,j,N_a}, d_{k,j,1}, \dots, d_{k,j,N_d}] \end{aligned} \quad (1)$$

N_a is the total number of active grid blocks in the reservoir model and N_d is the total number of data. The variables $\phi_{k,j,i}$, $kh_{k,j,i}$, $P_{k,j,i}$ and $S_{wk,j,i}$ are the porosity, horizontal permeability, pressure, and water saturation in grid block i , respectively; $d_{k,j,i}$ stands for the i -th reference production data, that is, BHP, SOR, or WCT for the six production wells. Function $trans$ defines a

transformation applied to state parameters, which ensures that these parameters still have physical values at the end of the updating step. These transformations are

1. Porosity $trans(\phi) = \log\left(\frac{\phi}{1-\phi}\right)$
2. Permeability $trans(kh) = \log(kh)$

Results for Production Data

We now compare the performance of the initial with the corrected models in terms of production data, that is, BHP, SOR, and WCT, and focus on two wells: well PRO-5 and well PRO-15 (Figures 5, 6). The production

responses are simulated for the two intervals previously described: the history-matching interval (0–2936 days) and the prediction interval (2936–6025 days). The limit between these two intervals is highlighted by the black dashed vertical line. The first column in each of the two graphs represents the BHP, the second column, the SOR, and the last one, the WCT. The first row in each graph corresponds to the initial ensemble, that is, the ensemble without any assimilation and the second row to the final ensemble, that is, the ensemble updated after all data assimilations. For the final ensemble, the updated model is taken back to day 0 and numerically simulated for the whole time span. In each graph, the gray curves show the production responses for each of the ensemble members, whereas the red curve corresponds to the reference model. The blue curves in the first and second rows correspond to production data obtained by the initial and final ensemble mean models, that is, porosity and permeability models, respectively.

Comparison of the two rows of Figures 5 and 6, respectively, stresses that the production responses simulated for the initial models fluctuate much more than those obtained for the corrected models. Moreover, the initial models do not follow the trend of the reference model, and the mean reservoir model derived from this initial ensemble behaves very differently than the reference model. However, after correction with the EnKF, the difference between the ensemble members and the reference model is reduced: the reference production data are now located in the range given by the ensemble members. In addition, the final mean reservoir model defined from the final ensemble reproduces the behavior of the reference model better than the initial ensemble mean model. For the two wells, the estimation of water breakthrough during the history-matching period is improved significantly compared with the initial ensemble. More specifically, starting from initial ensemble members that do not reproduce the reference WCT data, the assimilation with EnKF improves WCT results at least for well PRO-15: the WCT is fairly well captured by the corrected ensemble through the history-matching interval. However, the WCT match is still poor for well PRO-5. Matching WCT data, in general, is a difficult task because of its highly nonlinear dependence on model parameters.

In terms of the production responses, the corrected models provide reasonable predictions for BHP and SOR. As expected, the predicted WCTs are less reliable because the assimilation of the data during the history-matching phase led to smaller improvements. Overall, the updated ensemble outperforms the initial ensemble.

An indicator, which is widely used in the EnKF literature to quantify the quality of the updated model at each assimilation time in terms of history match

and prediction, is the root-mean-square (RMS) error. In this study, we refer to two different RMS error definitions. The first RMS error is denoted by $RMS_{d,1}$. At the end of each assimilation step, an average porosity and permeability model is determined from the mean of the ensemble members, then fluid flow is simulated for this average reservoir model during the whole history-matching interval (2936 days). The $RMS_{d,1}$ is defined as the error between the observed and simulated production data:

$$RMS_{d,1}(k) = \sqrt{\frac{1}{N_t} \sum_{i=1}^{N_t} \frac{1}{N_{data}^{t_i}} \sum_{j=1}^{N_{data}^{t_i}} (d_{obs}^j(t_i) - d_{mean,k}^j(t_i))^2} \quad (2)$$

In the equation, d stands for data such as BHP, SOR, and WCT; k is the assimilation time index; N_t is the number of data acquisition times up to and including time step k ; i is the time index; $N_{data}^{t_i}$ is the number of data collected at time, t_i , that is the number of wells; j is the data index; $d_{obs}^j(t_i)$ is the j^{th} data collected at time, t_i ; and $d_{mean,k}^j(t_i)$ is the j^{th} data simulated at time, t_i , for the mean reservoir model obtained after assimilation at time, t_k .

Figure 7 represents the evolution of the RMS value with time for BHP, SOR, and WCT. The choice of the initial ensemble may have an impact on the RMS results, especially for a small ensemble size. To take this effect into account, five ensembles of 50 members (among which is ensemble 1), updated with the same assimilation procedure, were used to calculate the RMS value. In all cases, the values are normalized to the initial RMS value. The RMS for BHP and SOR show a decreasing trend (except for ensemble 5), but the WCT RMS evolution is more chaotic. These results again stress the difficulty to match WCT compared matching BHP and SOR. Furthermore, our experiments have shown that when the ensemble size is increased to 100 or more, the differences between initial ensembles in terms of RMS results become less significant.

Results for Petrophysical Properties

Table 1 summarizes the properties of the porosity and permeability fields. Figures 8 and 9 display, for ensemble 1, the mean models derived from the initial porosity and permeability fields, respectively. They are almost uniform and equal to the porosity and permeability means, which are assumed to be stationary (Table 1).

By matching production data sequentially in time, heterogeneities and streaked features appear progressively in the porosity and permeability fields from one

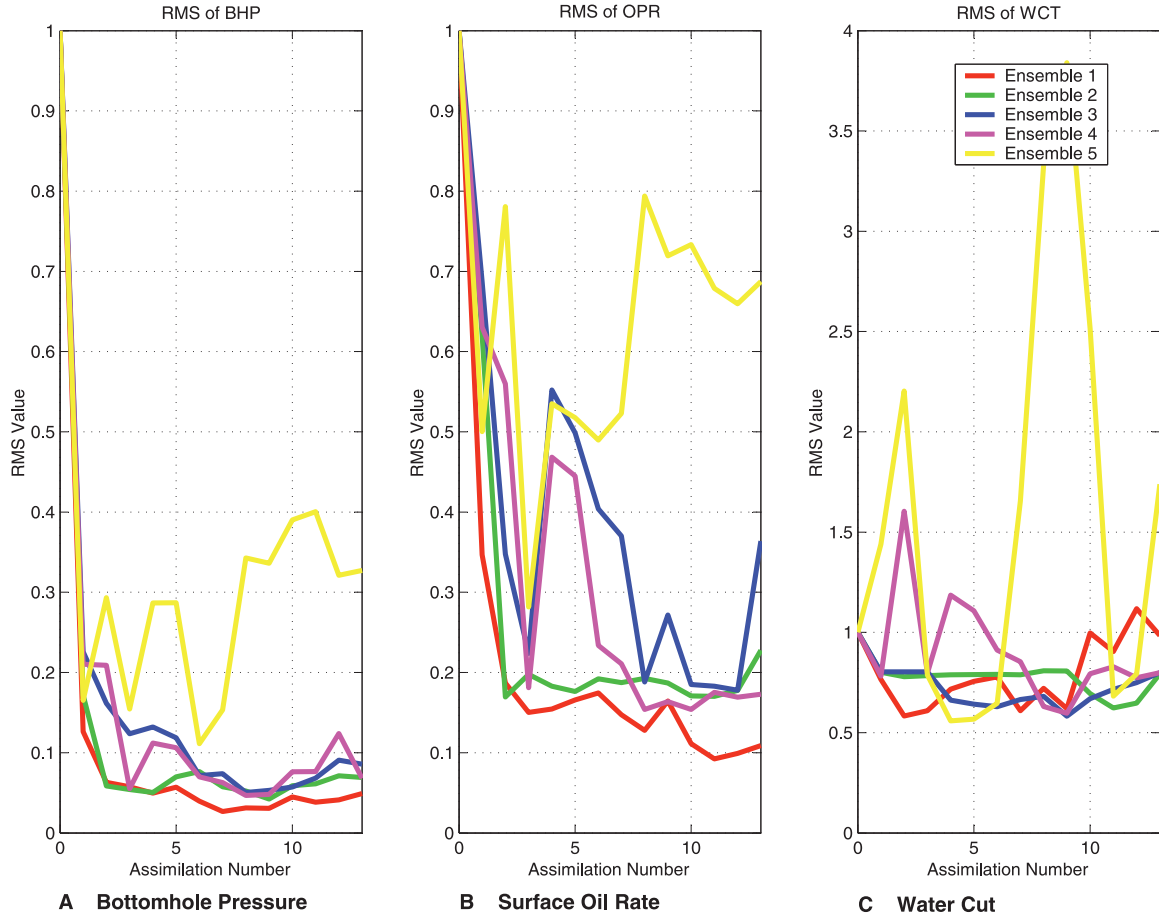


Figure 7. The first root-mean-square error ($RMS_{d,1}$) of production data. (A) Bottomhole pressure, (B) surface oil rate, and (C) water cut for five ensembles of size 50. The values are normalized on the initial value ($t = 0$).

assimilation time to the next. Figures 10 and 11 show the mean corrected porosity and permeability models after performing 13 assimilations, that is, 13 successive history matches of production data. The main features of the reference model (low- and high-porosity and permeability streaks in layers 1, 3, and 5, together with low- and high-porosity and permeability patches in layers 2 and 4) are retrieved in the corrected models. The porosity fields for layers 1, 3, and 5 were overestimated (the porosity values were expected to be lower than 0.35; they were trimmed when higher).

The overestimation is less significant for permeability fields; the updated fields are on the same order of magnitude as the reference model. Gao et al. (2006) related the overestimation problem to the constraints on well pressures and SORs in the fluid-flow simulation and reduced it by removing the bounds on the well BHP. This problem is mentioned in other applications of the EnKF (Gu and Oliver, 2005). According to Devegowda et al. (2007), the overestimation is a result of the spurious correlations in the covariance matrix because of the finite ensemble size. They proposed a mitigation

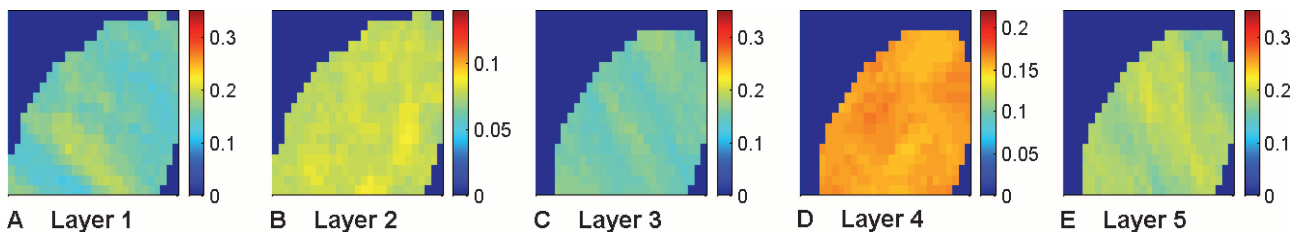


Figure 8. Mean of initial ensemble for porosity distribution in the five layers.

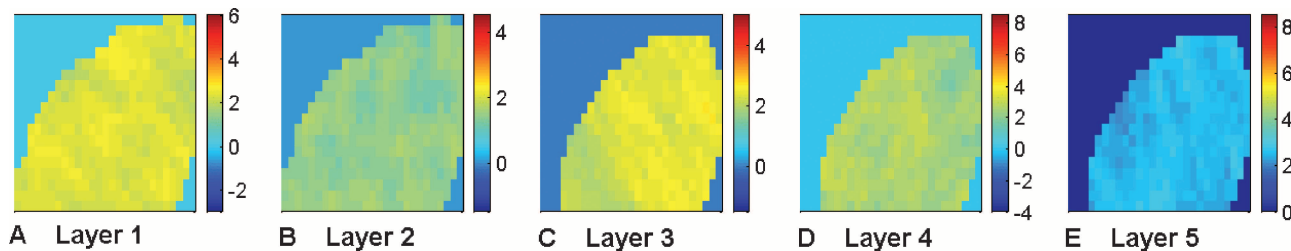


Figure 9. Mean of initial ensemble for permeability ($\ln[kh]$) distribution in the five layers.

strategy by covariance localization. This is beyond the scope of this chapter.

It can also be shown that the assimilation process induces a decrease in the variance of the porosity and permeability ensemble members, especially around well locations. As wells are perforated in layers 3, 4, and 5, variance reduction is more significant in these layers than in layers 1 and 2. Figures 12 and 13 display, for ensemble 1, the variance computed for the porosity and permeability models in layer 4. The first graph gives the variance for the initial ensemble, the middle one for the ensemble obtained after seven assimilations and the last one for the final ensemble (13 assimilations). Although variability reduction is a natural consequence of data assimilation, the updated ensemble should be representative of the variability of model parameters. Hence, excessive variance reduction should be avoided. This can be ensured using a larger ensemble. Moreover, the model noise is neglected in petroleum applications of the EnKF, and its inclusion may help mitigate this problem.

The distance between the assimilated porosity and permeability models for each ensemble member and the corresponding reference models is quantified by the following static RMS error:

$$RMS_s(k) = \sqrt{\frac{1}{N_e} \sum_{j=1}^{N_e} \frac{1}{N_a} \sum_{i=1}^{N_a} (y_{j,i} - y_{ref,i})^2} \quad (3)$$

Subscript s stands for static (reservoir parameters are regarded as static data), N_a is the number of active

grid blocks, i the grid block index, and j the ensemble member number. In addition, $y_{j,i}$ is the value of either the porosity or permeability logarithm attributed to the grid block i for the ensemble member j , and $y_{ref,i}$ is the reference value of this property. This RMS value quantifies the convergence toward the reference reservoir parameters or static data. Figure 14 shows, for ensemble 1, the static RMS values computed after each assimilation for porosity and horizontal permeability logarithm in the five layers (all values are normalized to the static RMS values computed at time 0). A decreasing trend is evident for most of the parameters, except for porosity in layers 1, 3, and 5. As previously explained, these layers control most of the flow, and their updated porosities were overestimated. The effect of the initial ensemble was also studied on the RMS value: although the RMS values are not the same for all ensembles, the same trend was observed for different ensembles of size 50.

SENSITIVITY ANALYSIS

The performance of EnKF for history match and prediction depends on several parameters, among which ensemble size, measurement data uncertainty, assimilation time step, and choice of the initial ensemble are important. A set of experiments illustrates the influence of these parameters on the results. To reduce the effect of the initial ensembles on the experiments dedicated to the influence of ensemble size, data uncertainty, and assimilation time step, five different

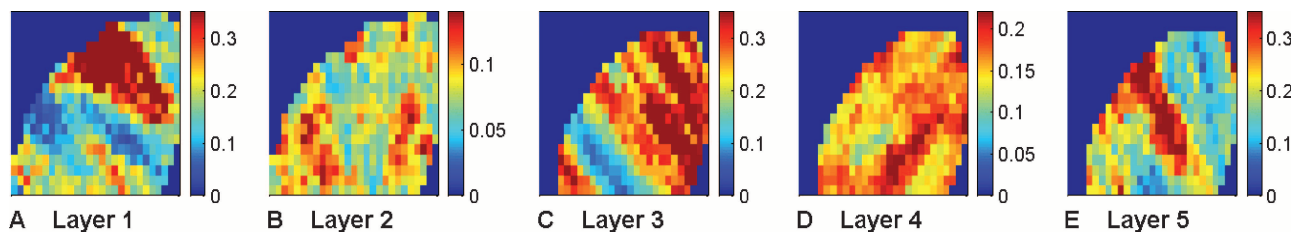


Figure 10. Mean of final ensemble for porosity distribution in the five layers.

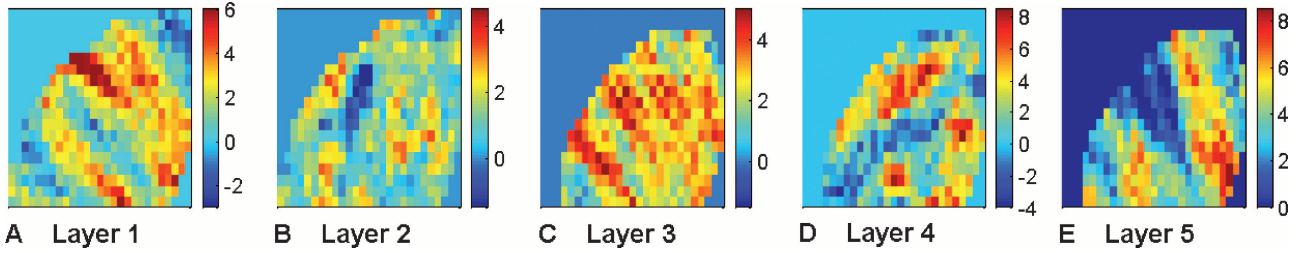


Figure 11. Mean of final ensemble for permeability ($\ln[kh]$) distribution in the five layers.

ensembles are generated for the target parameter, and the same assimilation process is performed for each of them. The RMS values presented hereafter are the average values of the RMS results obtained for the five ensembles.

Ensemble Size

The EnKF provides an approximation of the error covariance matrix from an ensemble of finite size. As the size of the ensemble, N_e , increases, the approximation of the error covariance matrix improves proportionally to $1/\sqrt{N}$. Therefore, spurious correlations in the covariance matrix are reduced. However, increasing the ensemble size induces a larger fluid-flow simulation and computational overburden. Thus, a trade-off exists between the accuracy of the covariance matrix approximation and the computational cost, and the choice of the ensemble size is case dependent. We apply the EnKF to the same case study as in the previous section but using ensembles of size 50, 100, 200, and 500. We consider the same data uncertainties as previously discussed. The assimilation intervals are reported by the red dashed vertical lines in Figure 4.

Two metrics quantify the performance of the different ensembles: the static RMS (RMS_s) previously introduced and the dynamic RMS, denoted by $RMS_{d,2}$. This quantity assesses the performance of EnKF at the end of each time step by calculating, for each of the ensemble members, the difference between the updated production responses (BHP, SOR, and WCT) and the

reference production data for the same time step. This RMS is written as

$$RMS_{d,2} = \sqrt{\frac{1}{N_e} \sum_{i=1}^{N_e} \frac{1}{N_t} \sum_{j=1}^{N_t} \frac{1}{N_{data}^{t_j}} \sum_{k=1}^{N_{data}^{t_j}} (d_{obs}^k(t_j) - d_i^k(t_j))^2} \quad (4)$$

N_e is the ensemble size. All other variables were previously defined. The $RMS_{d,2}$ value can be calculated for each of the target production responses BHP, SOR, or WCT separately, or for all of them together with respect to their uncertainties.

Table 2 provides the $RMS_{d,2}$ values determined for different ensemble sizes. The values are normalized to the average RMS obtained for the ensembles of size 50. At first glance, it seems that increasing the ensemble size from 50 to 100 decreases the RMS value. A larger increase in the ensemble size has a less significant effect. Therefore, an ensemble of size 100 is more appropriate considering central processing unit (CPU) costs.

Table 3 provides the RMS_s values for ensembles of increasing size. These values are normalized by the average RMS error determined for the ensembles of size 50. The larger the ensemble size, the lower the RMS error for most of the static properties. Furthermore, increasing the ensemble size from 200 to 500 reduces the static RMS error, but less so than when passing from 50 to 100 or 200. Thus, an ensemble of size 100 to 200 is well suited for the considered problem.

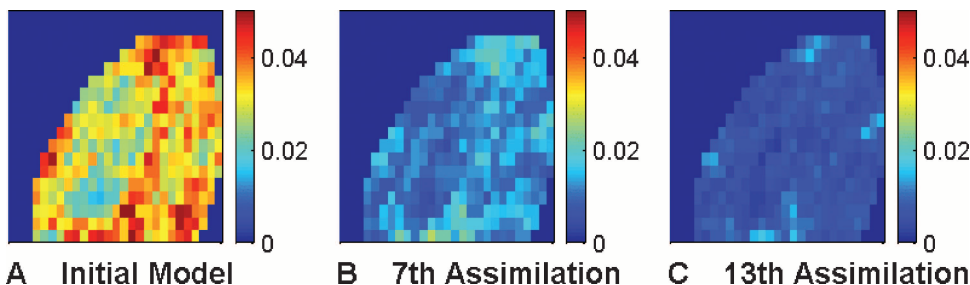
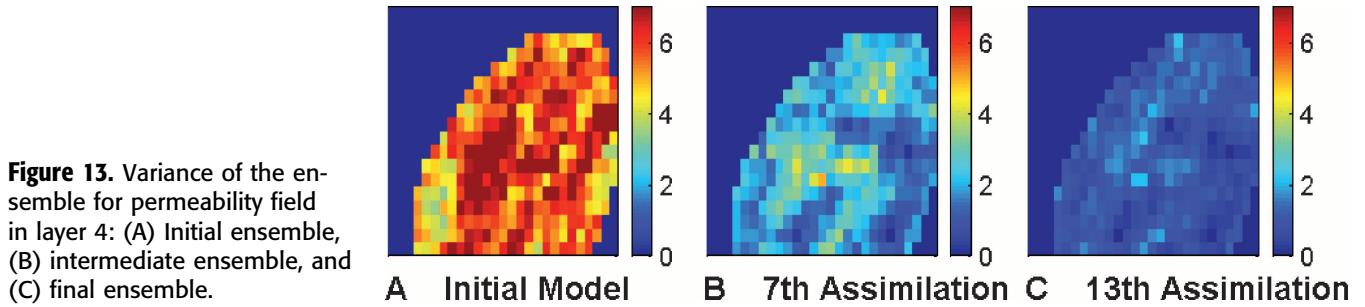


Figure 12. Variance of the ensemble for the porosity field in layer 4: (A) Initial ensemble, (B) intermediate ensemble, and (C) final ensemble.



Data Uncertainty

We now assess the effect of measurement uncertainty on the performance of the EnKF. Under the uncertainty 1 case, data uncertainties were set to 2 bars for BHP, 2 m³/day for SOR, and 0.02 for WCT. The uncertainty 2 case assumes an error of 3 bars for BHP, 3 m³/day for SOR, and 0.03 for WCT. The quality of the

results is again measured by the $RMS_{d,2}$ error (equation 4). The results presented in Table 4 are normalized to the average RMS value obtained for the ensembles of size 50 and the uncertainty 1 setting to make the comparison of results easier. In the uncertainty 2 configuration, the RMS errors computed for the production data are increased in comparison with uncertainty 1 for a given ensemble size. Apart from the ensembles of

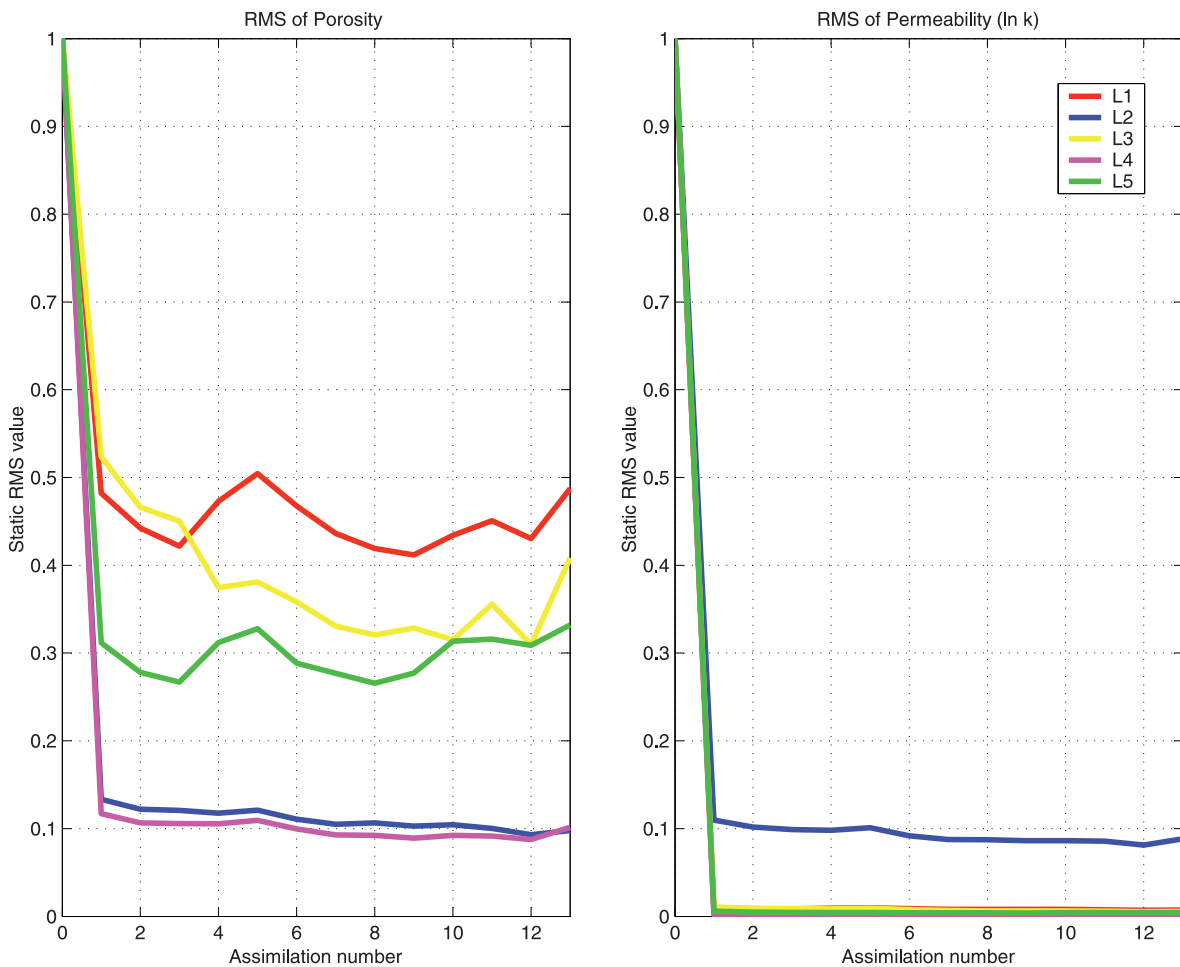


Figure 14. Static root-mean-square (RMS) values for the porosity and horizontal permeability log (ln[kh]) in layers 1 to 5. The values are normalized on the initial time ($t = 0$).

Table 2. Effect of ensemble size.*

Property	Ensemble Size			
	50	100	200	500
BHP**	1	0.33	0.27	0.25
SOR**	1	0.29	0.19	0.17
WCT**	1	0.44	0.44	0.41
All	1	0.34	0.30	0.26

*Average value of the dynamic $RMS_{d,2}$ obtained with several ensembles of increasing size, normalized on the value obtained with an ensemble size of 50.

**BHP = bottomhole pressure; SOR = surface oil rate; WCT = water cut.

size 50, our experiment demonstrates that even with a higher measurement of uncertainty, the final ensembles outperform the initial ensembles.

Haugen et al. (2008) have also performed a sensitivity test on measurement uncertainties for an application of the EnKF on a North Sea field case. They claimed that the choice of the measurement uncertainty is less important; assimilations with increased and decreased levels of uncertainty provided improved estimates compared with the initial reservoir models. They did not quantitatively compare the results.

Assimilation Step

The time interval between two consecutive assimilations is also an important issue for practical EnKF applications. Smaller assimilation steps may be required to capture significant perturbations or nonlinearities in fluid flow. These perturbations are induced by addition of a well or variations in flow rates.

Table 3. Effect of ensemble size.*

Property	Ensemble Size			
	50	100	200	500
Phi-L1	1	0.62	0.55	0.54
Phi-L2	1	0.74	0.68	0.66
Phi-L3	1	0.72	0.64	0.64
Phi-L4	1	0.67	0.64	0.65
Phi-L5	1	0.62	0.67	0.65
Ln(kh)-L1	1	0.67	0.66	0.61
Ln(kh)-L2	1	0.77	0.69	0.68
Ln(kh)-L3	1	0.83	0.69	0.72
Ln(kh)-L4	1	0.81	0.77	0.74
Ln(kh)-L5	1	0.71	0.71	0.65

*Average value of the static root-mean-square obtained with several ensembles of increasing size, normalized on the value obtained with an ensemble size of 50.

Table 4. Effect of measurement uncertainty.*

Ensemble size	Uncertainty 1			Uncertainty 2		
	50	100	200	50	100	200
BHP**	1	0.33	0.27	1.26	0.70	0.61
SOR**	1	0.29	0.19	1.11	0.49	0.37
WCT**	1	0.44	0.44	1.02	0.98	0.96
All	1	0.34	0.30	1.11	0.62	0.54

*Average value of the dynamic $RMS_{d,2}$ obtained with two increasing levels of uncertainty and several ensembles of increasing size, normalized on the value obtained with an ensemble size of 50.

**BHP = bottomhole pressure; SOR = surface oil rate; WCT = water cut.

The production scheme followed for this case study involves several changes in the flow rate. Therefore, we compare the performance of the EnKF for two distinct time step settings. The first assimilation time partitioning, time step 1, is reported in Figure 4. In the second partitioning, time step 2, each of the previous time steps is divided in two smaller steps. We considered ensembles of size 50, 100, and 200 for the uncertainty 1 metric.

Results are compared using the $RMS_{d,2}$ error metric (equation 4). The RMS errors reported in Table 5 are normalized to the average RMS values determined for the ensembles of size 50 with the time step 1 setting. Keeping the ensemble size constant while decreasing the time step size makes the RMS smaller for the target production responses. Also, decreasing the time step size while increasing the ensemble size contributes even more to improve the match.

Choice of the Initial Ensemble

One of the main issues with EnKF is the choice of the initial ensemble because different initial ensembles result in different RMS values for production data,

Table 5. Effect of assimilation interval.*

Ensemble size	Time Step 1			Time Step 2		
	50	100	200	50	100	200
BHP**	1	0.33	0.27	0.60	0.28	0.24
SOR**	1	0.29	0.19	0.56	0.21	0.15
WCT**	1	0.44	0.44	0.50	0.35	0.29
All	1	0.34	0.30	0.54	0.27	0.22

*Average value of the dynamic $RMS_{d,2}$ obtained with two decreasing sets of assimilation time intervals and several ensembles of increasing size, normalized on the value obtained with an ensemble size of 50.

**BHP = bottomhole pressure; SOR = surface oil rate; WCT = water cut.

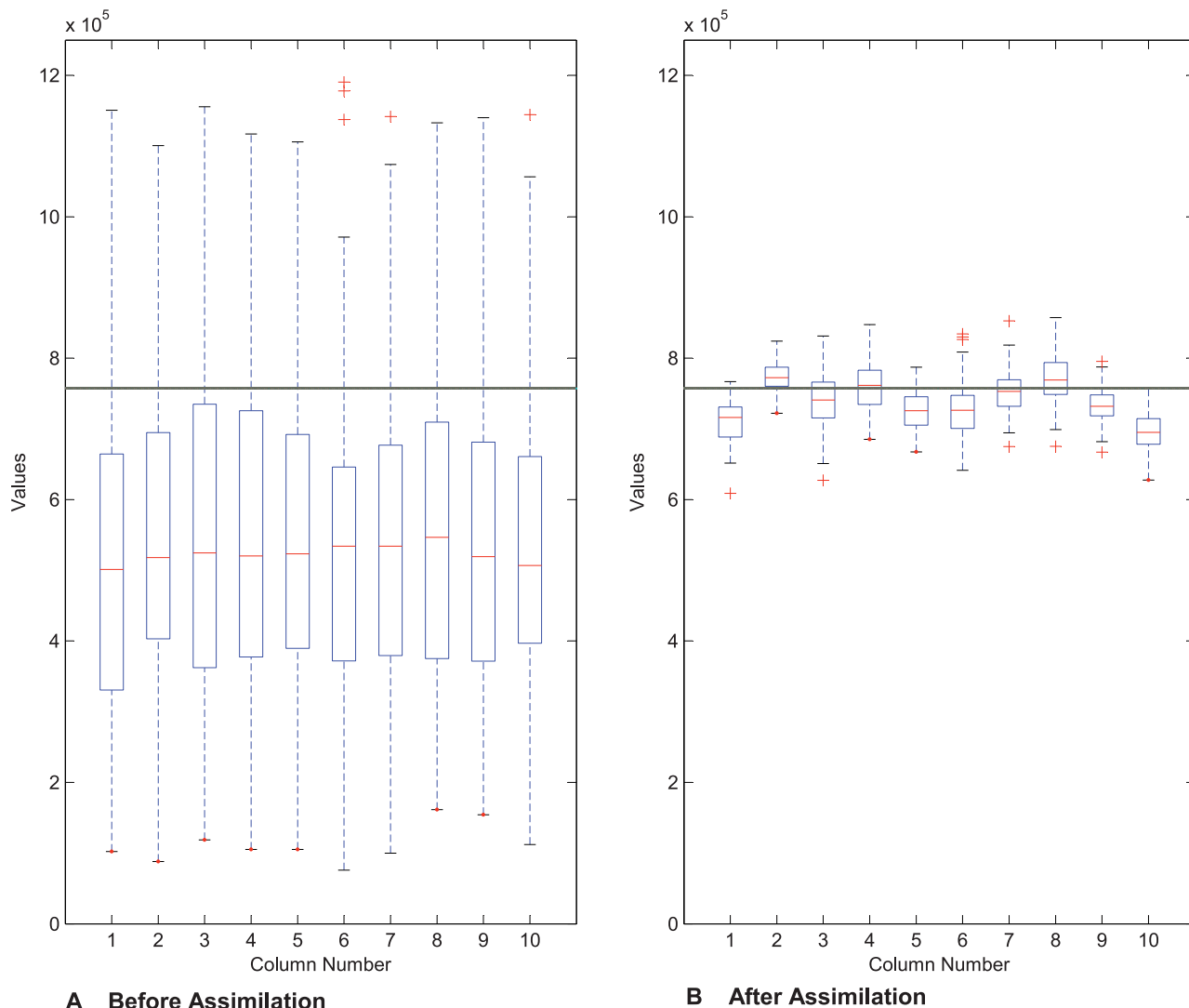


Figure 15. Box plot of cumulative oil production for 10 ensembles of size 100: (A) initial ensemble, (B) final ensemble. The black horizontal line corresponds to the cumulative oil production for the reference reservoir model at the end of 6025 days of production. Each box is limited by the lower and upper quartiles, and the red line within each box shows the median value. The small black lines (whiskers) show the extent of the data for each box plot. Red plus signs are outliers of each data set.

indicating the importance of the initial ensemble in the quality of history match and predictions. Initial ensembles are generated stochastically and filter performance may change from one ensemble to another (Lorentzen et al., 2005). Moreover, ensemble members become highly correlated after assimilation. This phenomenon is a well-known problem of Markov Chain–Monte Carlo methods. To mitigate these limitations, Thulin et al. (2008) recommended performing several EnKF runs with an appropriate small ensemble size and claimed that the results would be superior to those obtained by only one large ensemble.

How does the EnKF perform in terms of prediction capability with different ensembles of identical size?

Focusing on cumulative oil production, ten different ensembles of size 100 were generated using the uncertainty 1 and time step 1 framework. The forecast capability of each of the ensembles is assessed by comparing the total cumulative oil production from the initial value with that of the final updated ensembles for the whole history-matching and prediction intervals. To make the comparison meaningful, the updated models obtained at the end of the history-matching interval (0–2936 days) were simulated from day 0 to the end of the prediction interval. The results are plotted in Figure 15.

The reference oil data are in the range provided by the initial ensembles, more specifically between the

upper quartile and the upper extent for the data. The median predicted oil cumulative production is far from the true one and the spread, that is, P(75) to P(25), for each ensemble is fairly high. After assimilating the data in the history-matching interval, the spread is reduced and the true cumulative oil production value is better positioned within the forecasted ranges. Moreover, the difference between the median and true cumulative oil production is significantly smaller, and one-half of the ensembles include the true value between the lower and upper quartiles, that is, P(75) to P(25). Considering the range of predictions by the 10 ensembles, we suggest that sound predictions should be based on several ensembles of appropriate size, similar to what was suggested by Lorentzen et al. (2005) and Thulin et al. (2008).

CONCLUSIONS

The ease of implementation and low computational cost make the EnKF method appealing for most history-matching studies. Although the applications are generally successful, the fundamental assumptions intrinsic to EnKF theory may be problematic, although mitigation strategies were suggested in the literature to improve the performance. In this chapter, we focus on the use of the EnKF method for performing history match and uncertainty quantification. A fairly small ensemble of size 50 is used to provide the initial uncertainty in porosity and permeability. By sequentially matching the production data (BHP, SOR, and WCT), porosity and permeability fields were gradually adjusted so as to reproduce the reference production data. The WCT was shown to be quite difficult to match possibly because of the highly nonlinear dependence of these data to reservoir parameters.

We also performed a set of sensitivity tests to assess the function of some EnKF parameters in history-matching results: the ensemble size, the data uncertainty, the assimilation time step, and the choice of the initial ensemble. The following conclusions can be drawn:

1. Increasing the ensemble size results in a better match for the production data (BHP, SOR, and WCT), but there exists a trade-off between the increase in computation time and the improvements in the results. Our experiments suggest that an ensemble size of 100 to 200 is appropriate to obtain acceptable results with EnKF. However, this number is case dependent.
2. The level of uncertainty in measured data is of less significance; data assimilation with EnKF improves model estimates whenever the size of the ensemble is large enough.
3. Decreasing the assimilation time step is required to better capture the abrupt changes in dynamics of the model.
4. The match of cumulative oil production is better assessed when estimated from several ensembles of identical size, although this makes the process more CPU time consuming.

REFERENCES CITED

- Anderson, J. L., 2001, An ensemble adjustment filter for data assimilation: *Monthly Weather Review*, v. 129, p. 2884–2903, doi:10.1175/1520-0493(2001)129<2884:AEAKFF>2.0.CO;2.
- Anderson, J. L., 2007, Exploring the need for localization in ensemble data assimilation using a hierarchical ensemble filter: *Physica D*, v. 230, p. 99–111, doi:10.1016/j.physd.2006.02.011.
- Aziz, K., and A. Settari, 1979, *Petroleum reservoir simulation*: London, U.K., Applied Science, 497 p.
- Bertino, L., G. Evensen, and H. Wackernagel, 2003, Sequential data assimilation techniques in oceanography: *International Statistical Review*, v. 71, no. 2, p. 223–241, doi:10.1111/j.1751-5823.2003.tb00194.x.
- Burgers, G., P. J. van Leeuwen, and G. Evensen, 1998, Analysis scheme in the ensemble Kalman filter: *Monthly Weather Review*, v. 126, p. 1719–1724, doi:10.1175/1520-0493(1998)126<1719:ASITEK>2.0.CO;2.
- Chen, Y., D. S. Oliver, and D. Zhang, 2009, Data assimilation for nonlinear problems by ensemble Kalman filter with reparameterization: *Journal of Petroleum Science and Engineering*, v. 66, p. 1–14, doi:10.1016/j.petrol.2008.12.002.
- Cohn, S. E., 1997, An introduction to estimation theory: *Journal of the Meteorological Society of Japan*, v. 75, p. 257–288.
- Devegowda, D., E. Arroyo-Negrete, A. Datta-Gupta, and S. G. Douma, 2007, Efficient and robust reservoir model updating using ensemble Kalman filter with sensitivity-based covariance localization: *SPE Reservoir Simulation Symposium*, February 26–28, 2007, Houston, Texas, SPE paper 106144, 14 p.
- Evensen, G., 1994, Sequential data assimilation with a nonlinear quasi-geostrophic model using Monte Carlo methods to forecast error statistics: *Journal of Geophysical Research Ocean*, v. 99, no. C5, p. 10,143–10,162, doi:10.1029/94JC00572.
- Evensen, G., 2007, *Data assimilation: The ensemble Kalman filter*: Berlin, Germany, Springer, 307 p.
- Evensen, G., and P. J. van Leeuwen, 1996, Assimilation of geosat altimeter data for the Agulhas current using the ensemble Kalman filter with a quasigeostrophic model: *Monthly Weather Review*, v. 124, p. 85–96, doi:10.1175/1520-0493(1996)124<0085:AOGADF>2.0.CO;2.
- Evensen, G., H. Hove, H. C. Meisingset, E. Reiso, and Ø.

- Espelid, 2007, Using the EnKF for assisted history matching of a North Sea reservoir model: SPE Reservoir Simulation Symposium, February 26–28, 2007, Houston, Texas, SPE paper 106184, 13 p.
- Fertig, E., B. R. Hunt, E. Ott, and I. Szunyogh, 2007, Assimilating nonlocal observations with a local ensemble Kalman filter: *Tellus*, v. 59A, p. 719–730.
- Floris, F. J. T., M. D. Bush, M. Cuypers, F. Roggero, and A. R. Syversveen, 2001, Methods for quantifying the uncertainty of production forecasts: A comparative study: *Petroleum Geoscience*, v. 7, p. 87–96.
- Gao, G., M. Zafari, and A. C. Reynolds, 2006, Quantifying uncertainty for the PUNQ-S3 problem in a Bayesian setting with RML and EnKF: *SPE Journal*, v. 11, no. 4, p. 506–515.
- Gu, Y., and D. S. Oliver, 2005, History Matching of the PUNQ-S3 reservoir model using the ensemble Kalman filter: *SPE Journal*, v. 10, p. 217–224.
- Gu, Y., and D. S. Oliver, 2007, An iterative ensemble Kalman filter for multiphase fluid flow data assimilation: *SPE Journal*, v. 12, no. 4, p. 438–446.
- Hamill, T. M., and J. S. Whitaker, 2001, Distance-dependent filtering of background error covariance estimate in an ensemble Kalman filter: *Monthly Weather Review*, v. 129, p. 2776–2790, doi:10.1175/1520-0493(2001)129<2776:DDFOBE>2.0.CO;2.
- Haugen, V., and G. Evensen, 2002, Assimilation of SLA and SST data into OGCM for the Indian Ocean: *Ocean Dynamics*, v. 52, p. 133–151, doi:10.1007/s10236-002-0014-7.
- Haugen, V., L. Natvik, G. Evensen, A. Berg, K. Flornes, and G. Naevdal, 2008, History matching using the ensemble Kalman filter on a North Sea field case: *SPE Journal*, v. 13, no. 4, p. 382–391.
- Houtekamer, P., and H. L. Mitchell, 1998, Data assimilation using an ensemble Kalman filter technique: *Monthly Weather Review*, v. 126, no. 3, p. 796–811, doi:10.1175/1520-0493(1998)126<0796:DAUAEK>2.0.CO;2.
- Houtekamer, P., and H. L. Mitchell, 2001, A sequential ensemble Kalman filter for atmospheric data assimilation: *Monthly Weather Review*, v. 129, p. 123–137, doi:10.1175/1520-0493(2001)129<0123:ASEKFF>2.0.CO;2.
- Kalman, R. E., 1960, A new approach to linear filtering and prediction problems: *Transactions of the American Society of Mechanical Engineers—Journal of Basic Engineering*, v. 82, p. 35–45.
- Le Ravalec, M., B. Noetinger, and L. Y. Hu, 2000, The FFT moving average (FFT-MA) generator: An efficient numerical method for generating and conditioning Gaussian simulations: *Mathematical Geology*, v. 32, no. 6, p. 701–723, doi:10.1023/A:1007542406333.
- Li, G., and A. C. Reynolds, 2007, An iterative ensemble Kalman filter for data assimilation: SPE Annual Technical Conference and Exhibition, November 11–14, 2007, Anaheim, California, SPE paper 109808, 18 p.
- Liu, N., and D. S. Oliver, 2005, Critical evaluation of the ensemble Kalman filter on history matching of geologic facies: *SPE Reservoir Evaluation and Engineering*, v. 8, no. 6, p. 470–477.
- Lorenc, A. C., 1986, Analysis methods for numerical weather prediction: *Quarterly Journal of the Royal Meteorological Society*, v. 112, no. 474, p. 1177–1194, doi:10.1002/qj.49711247414.
- Lorentzen, R. J., G. Naevdal, B. Valles, A. N. Berg, and A. A. Grimstad, 2005, Analysis of the ensemble Kalman filter for estimation of permeability and porosity in reservoir models: SPE Annual Technical Conference and Exhibition, October 9–12, 2005, Dallas, Texas, SPE paper 96375, 10 p.
- Margulis, S. A., D. McLaughlin, D. Entekhabi, and S. Dunne, 2002, Land data assimilation and estimation of soil moisture using measurements from the Southern Great Plains 1997 field experiment: *Water Resources Research*, v. 38, no. 12, p. 35.1–35.18.
- Moreno, D., S. I. Aanonsen, G. Evensen, J. A. Skjervheim, 2008, Channel facies estimation based on Gaussian perturbations in the EnKF: European Association of Geoscientists and Engineers 11th European Conference on the Mathematics of Oil Recovery, September 8–11, 2008, Bergen, Norway.
- Naevdal, G., T. Mannseth, and E. H. Vefring, 2002, Near-well reservoir monitoring through ensemble Kalman filter: SPE/DOE Improved Oil Recovery Symposium, April 13–17, 2002, Tulsa, Oklahoma, SPE paper 75235, 9 p.
- PumaFlow, 2007, Reference Manual Release 2.0, September, BeicipFranlab–Institut Français du Pétrole.
- PUNQ-S3 test case, 2010: <http://www3.imperial.ac.uk/earthscienceandengineering/research/perm/punq-s3model/onlinedataset> (accessed May 1, 2009).
- Thulin, K., G. Naevdal, and S. I. Aanonsen, 2008, Quantifying Monte Carlo uncertainty in the ensemble Kalman filter: 11th European Conference on the Mathematics of Oil Recovery, September 8–11, 2008, Bergen, Norway.
- Vabø, J. G., G. Evensen, J. Hove, and J. A. Skjervheim, 2008, Using the EnKF with kernel methods for estimation of non-Gaussian variables: European Association of Geoscientists and Engineers 11th European Conference on the Mathematics of Oil Recovery, September 8–11, 2008, Bergen, Norway.
- Wang, X., T. M. Hamill, J. S. Whitaker, and C. H. Bishop, 2007, A comparison of hybrid ensemble transform Kalman filter: Optimum interpolation and ensemble square root filter analysis schemes: *Monthly Weather Review*, v. 135, no. 3, p. 1055–1076, doi:10.1175/MWR3307.1.
- Wen, X.-H., and W. H. Chen, 2007, Some practical issues on real-time reservoir model updating using ensemble Kalman filter: *SPE Journal*, v. 12, no. 2, p. 156–166.
- Wunsch, C., 1996, *The ocean circulation inverse problem*: New York, Cambridge University Press, 437 p.
- Zafari, M., and A. C. Reynolds, 2007, Assessing the uncertainty in reservoir description and performance predictions with the ensemble Kalman filter: *Society of Petroleum Engineering Journal*, v. 12, no. 3, p. 382–391.